Hindawi
Journal of Sensors
Volume 2017, Article ID 7692491, 9 pages
https://doi.org/10.1155/2017/7692491

Research Article

Design and Test of Portable Hyperspectral Imaging Spectrometer

Chunbo Zou,[1,2] Jianfeng Yang,[1] Dengshan Wu,[1] Qiang Zhao,[1] Yuquan Gan,[1] Di Fu,[1] Fanchao Yang,[1] Hong Liu,[1] Qinglan Bai,[1] and Bingliang Hu[1]

[1] *Xi'an Institute of Optics and Precision Mechanics, Chinese Academy of Sciences, Xi'an 710119, China*
[2] *University of Chinese Academy of Sciences, Beijing 10049, China*

Correspondence should be addressed to Chunbo Zou; zouchb@opt.ac.cn

Received 16 March 2017; Revised 10 July 2017; Accepted 16 July 2017; Published 27 August 2017

Academic Editor: Jesus Corres

We design and implement a portable hyperspectral imaging spectrometer, which has high spectral resolution, high spatial resolution, small volume, and low weight. The flight test has been conducted, and the hyperspectral images are acquired successfully. To achieve high performance, small volume, and regular appearance, an improved Dyson structure is designed and used in the hyperspectral imaging spectrometer. The hyperspectral imaging spectrometer is suitable for the small platform such as CubeSat and UAV (unmanned aerial vehicle), and it is also convenient to use for hyperspectral imaging acquiring in the laboratory and the field.

1. Introduction

Hyperspectral imaging spectrometer can acquire hundreds of inhomogeneous spectral images. Compared to the other sensors, much more information could be excavated from the massive data. Owing to the characters above, the demand for the hyperspectral imaging spectrometer is put forward in many different tasks such as accurate mapping of wide areas, target detection, process monitoring and control, object identification and recognition, clinical diagnosis imaging, and environment assessment and management. After decades of development, the application areas of the hyperspectral imaging spectrometer have extended to ecology, geology, agriculture, medicine, military, security, oceanography, manufacturing, urban studies, and others [1–4].

With the development of machinery and electronics technology [5], the unmanned aerial vehicle (UAV) and the CubeSat have made great progress. Due to the miniaturization of platform, the small, compact, portable hyperspectral imaging spectrometer becomes a development direction [6–9].

In this paper, we design and implement a portable hyperspectral imaging spectrometer. Using the hyperspectral imaging spectrometer, we conduct the flight test experiment and acquire the hyperspectral image of the bared soil, roofs, green wheat, and so on.

The final implemented hyperspectral imaging spectrometer can provide an instantaneous FOV of 0.22 mrad in 6.57 degrees and a spectral sampling of 1.6 nm and covers the range of 450 to 850 nm.

2. Considerations and Design Specifications

The hyperspectral imaging spectrometer designed and implemented in the paper is used for acquiring experimental hyperspectral imaging data in the field and laboratory. Another application is used for remote sensing installed in the small platform such as UAV and CubeSat.

To be suited for the small platform and the convenience of the field experiment, the hyperspectral imaging spectrometer must have a small volume, a light weight, and a regular appearance.

Two forms of the instrument are considered, the whiskbroom sensor and the pushbroom sensor. The whiskbroom sensor can achieve the highest spectral and spatial uniformity. However, the whiskbroom sensor records the spectrum of every point on a single linear detector array. The pushbroom

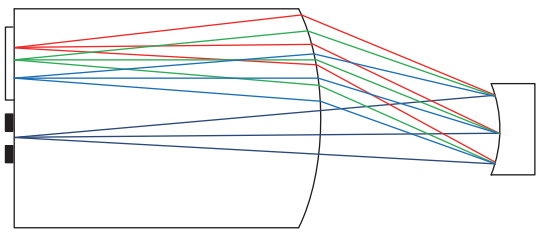

Figure 1: The Dyson spectrometer.

sensor disperses the image of a slit onto a two-dimensional array detector. It is clear that the efficiency of the pushbroom sensor is much higher than the whiskbroom sensor. Thus the pushbroom imaging spectrometers are becoming a preferred form for many remote and laboratory sensing applications. The typical pushbroom imaging spectrometer consists of a telescope, a slit, a dispersing spectrometer, and an array detector.

There are many methods to achieve the dispersing spectrometer of the pushbroom hyperspectral imaging spectrometer. For high performance and compact structure, the Dyson structure is utilized, as is shown in Figure 1. In 1959, Dyson first proposed that a simple concentric arrangement of a planoconvex lens and concave mirror would be free of all Seidel aberrations at the design wavelength and center of a field imaged at 1 : 1 magnification [10]. Since then, many papers have advanced the concept to fully working systems [11]. In recent years, lots of research institutions develop many compact spectrometer based on the Dyson structure [12–17]. The advantageous features of this particular concentric configuration are as follows: (1) sharp imagery due to the inherent absence of Seidel aberrations; (2) high numerical aperture; (3) flat field; (4) wide unvignetted field having linear dispersion as a function of wavelength; (5) nonanamorphic field; (6) telecentric; (7) no central obscuration of the pupil; (8) no aspherical optical surfaces being required [18, 19].

Based on the above considerations, we design a high resolution hyperspectral imaging spectrometer in both spectral dimension and spatial dimension. The specifications are presented in Table 1.

3. Optical Design

To prove the advantages of the system above, we design and implement the hyperspectral imaging spectrometer.

3.1. Telescope Design. The telescope is designed using a refraction system. The specifications are shown in Table 2.

We use three kinds of glasses from the CDGM material catalogs of ZEMAX: CAF2, H-LAK2A, and TF3. The telescope is designed as Figure 2, the total length of the telescope is 95.9 mm, and the stop is at the first glass of the system whose diameter is 13.2 mm. The exit pupil position is −20000 mm from the image surface.

It can be seen that the MTF is higher than 0.75 at the Nyquist frequency (67.6 lp/mm) of the sensor from Figure 3.

The energy is included mostly in the pixel range from the spot diagram shown in Figure 4, and the RMS of the spot diagram is 1.754 μm. The distortion is less than 0.27% shown in Figure 5.

Table 1: Design specifications.

Parameter	Value
Principle	Pushbroom
Spectral range (nm)	450–850
Spectral sampling (nm)	1.6
Field of view (degrees)	6.57
Instantaneous FOV (mrad)	0.22
F-number	2.5
Pixel size (μm)	7.4
Spatial swath (pixels)	1024
Spectral pixels	512
Slit width (μm)	13.2

Table 2: Telescope specifications.

Parameter	Value
Working range (nm)	450–850
Focal length (mm)	66
Field of view (degrees)	>6.6°
F-number	2.5
Other demand	Telecentric

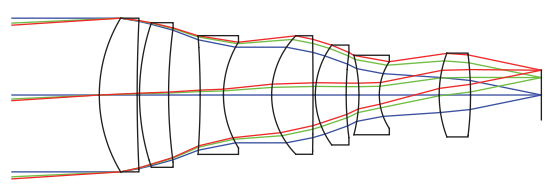

Figure 2: Ray trace of the telescope.

3.2. Spectrometer Design. The Dyson spectrometer is compact and has high performances. But if we use the prototype, there is no space to install the array detector and the mechanical slit shown in Section 4. For the regular appearance of the system and to avoid the overlapping of the slit assembly and the detector, we design a new form of the Dyson spectrometer based on the prototype.

First, we separate the object surface and the image surface of the spectrometer along the optical axis. A meniscus lens is added before the concave grating to correct the aberration brought by the separation at the same time, as is shown in Figure 6.

Second, we add a reflective surface to the Dyson block; the dispersing light is reflected to the bottom of the system and then received by the detector, as is shown in Figure 7. The slit and the detector are successfully separated to the two perpendicular surfaces. The Dyson block is shown in Figure 8.

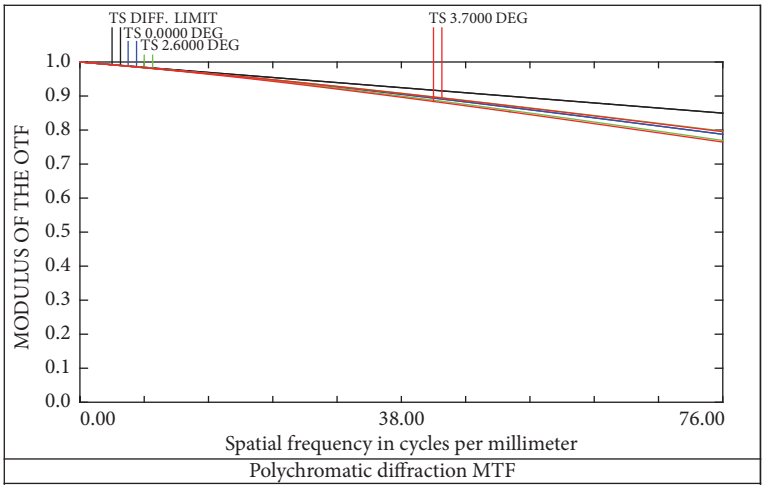

Figure 3: MTF of the telescope.

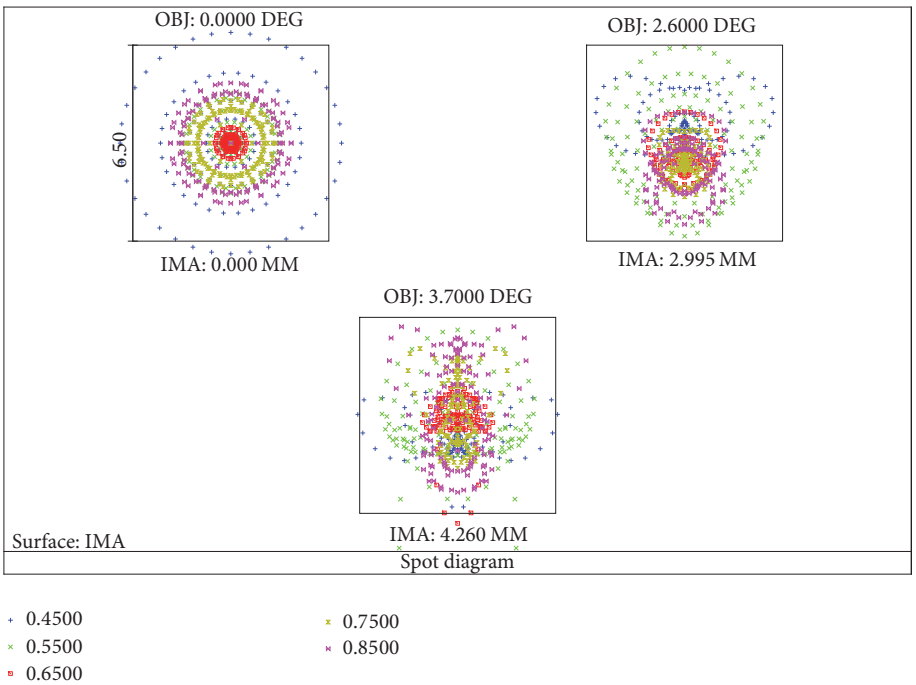

Figure 4: Ensquared energy of the telescope.

The material of the Dyson block and the meniscus lens is H-K9L in the CDGM glass catalog, which has the same parameters as the N-BK7 of SCHOTT. In the Dyson block, the thickness is 50.23 mm, radius is 53.46 mm, the distance between the left endpoint of the reflect surface and the axis is 1.4 mm, and the angle between the reflective surface and the axis is 45°. The radii of the meniscus lens are 337.3 mm and 398.1 mm and the thickness of the meniscus lens is 6 mm. The concave grating is a holographic Rowland grating, whose groove density is 83 lines/mm and radius is 173.9 mm. The distance between the Dyson block and the meniscus lens is 105.45 mm, and the distance between the meniscus lens and the grating is 6 mm.

3.3. Simulation of the Hyperspectral Imaging Spectrometer. The ray trace of the hyperspectral imaging spectrometer is shown in Figure 9. The total length of the system is 246.7 mm, and the largest diameter is 47.4 mm.

The matrix spot diagram shows that the spots diagram of all waves are less than the width of the slit (13.2 μm) (Figure 10).

At the maximal field of the hyperspectral imaging spectrometer, the maximal distortion is 0.32% occurring in the 450 nm wavelength, and the minimal distortion is 0.22% occurring in the 850 nm wavelength. Thus the keystone of the system could be calculated as follows: 0.32% − 0.22% = 0.1% (Figure 11).

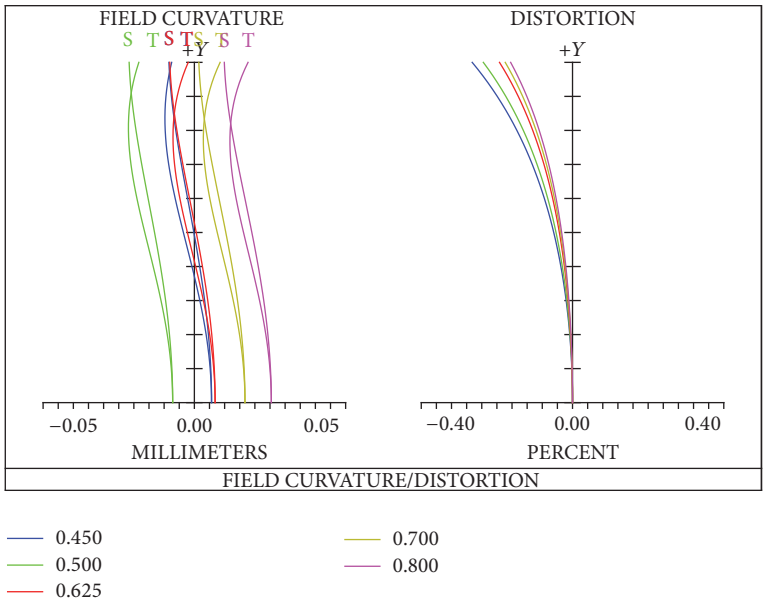

Figure 5: Distortion of the telescope.

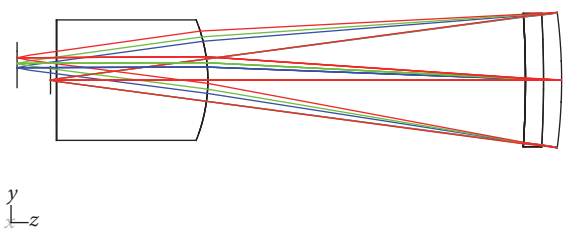

Figure 6: Ray trace of the first step of the design of the spectrometer.

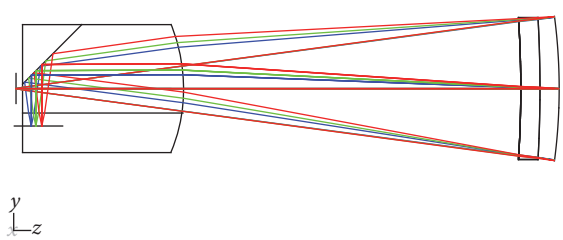

Figure 7: Ray trace of the second step of the design of the spectrometer.

Figure 8: The Dyson block.

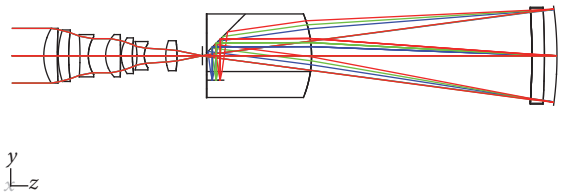

Figure 9: Simulation of the hyperspectral imaging spectrometer.

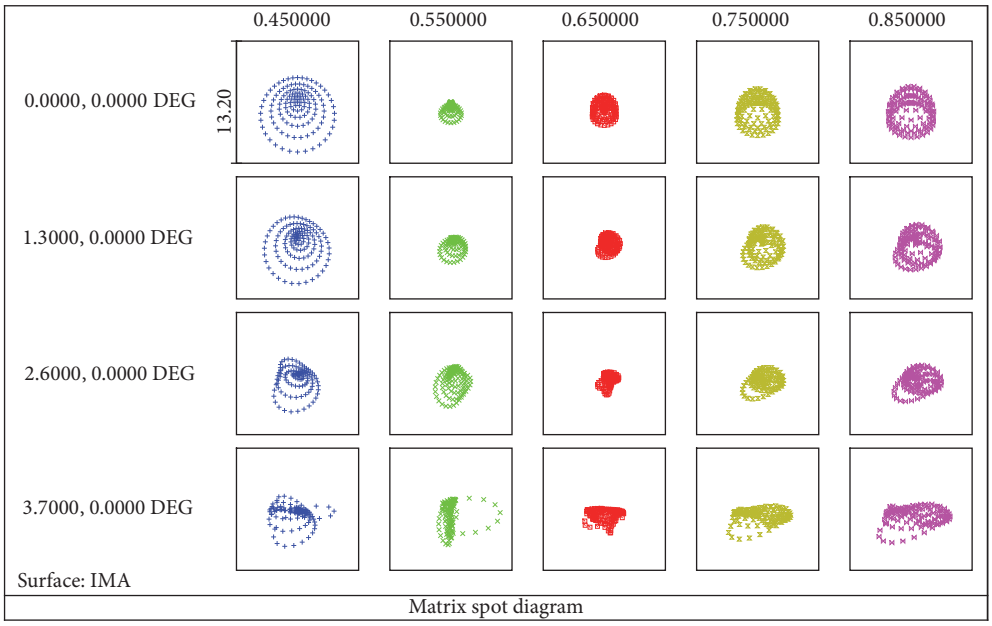

Figure 10: Matrix spot diagram of the hyperspectral imaging spectrometer.

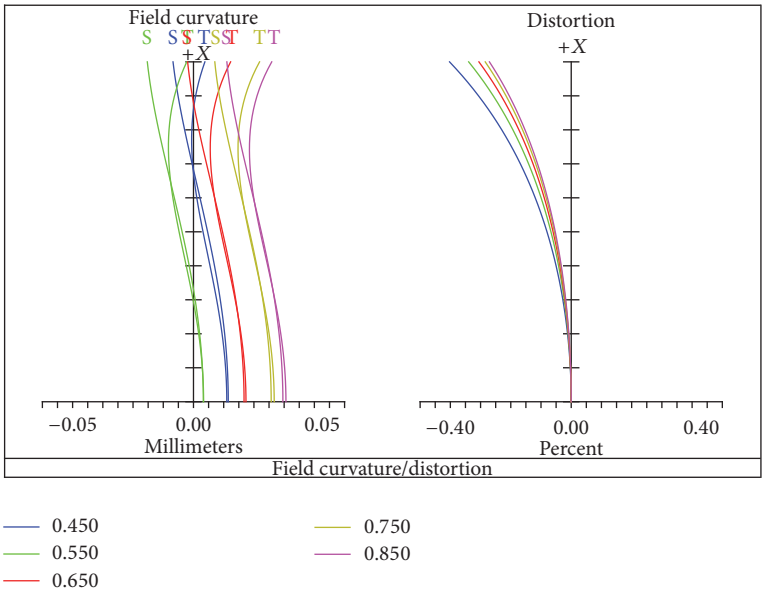

Figure 11: Distortion (keystone) of the spectrometer.

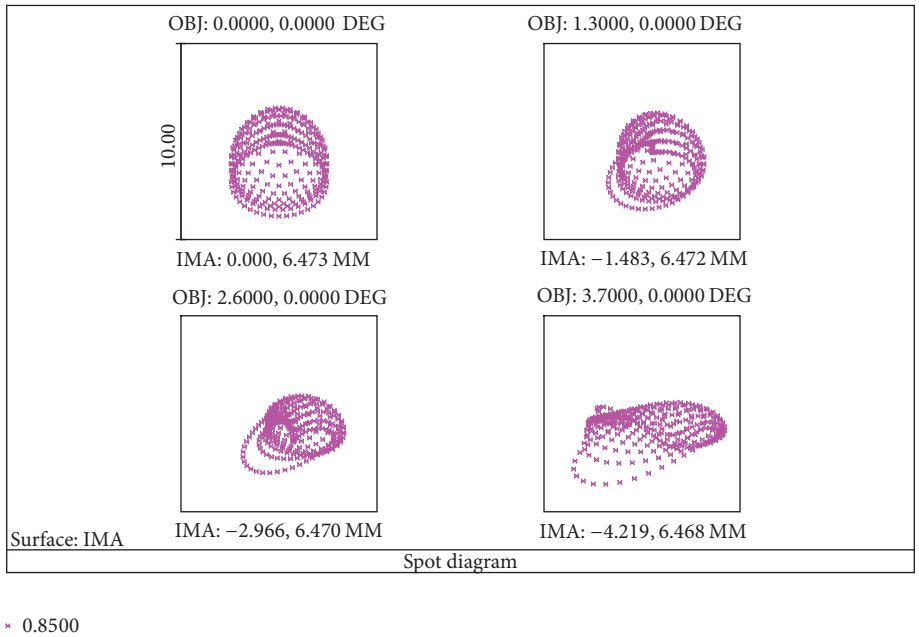

Figure 12: The smile of the hyperspectral imaging spectrometer at 850 nm.

The maximal smile of the hyperspectral imaging spectrometer occurs in the wavelength of 850 nm, which could be got from Figure 12: 6.473 mm − 6.468 mm = 0.005 mm.

4. Slit Assembly

The slit assembly is a critical element of the overall design. It could be accomplished with a lithographic technique that creates the slit on a silicon nitride membrane supported on a Si wafer [20], and it could also be made by two mechanical blades installed on the base and adjusted accurately under the microscope.

The slit accomplished by the lithographic technique is straight and uniform within 100 nm or better, but the Si wafer has a high reflection and would amplify the stray light if measures are not taken, because light reflected from the detector is returned toward the slit at high efficiency and can then be redirected toward the spectrometer.

The slit made by two mechanical blades can absorb the light reflected by the detector because the mechanical blade is dyed black. And it is used to implement the instrument in the paper, as is shown in Figure 13.

5. Focal Plane Array

The hyperspectral imaging spectrometer utilizes a CMOS camera of the DALSA Corporation. The specifications of the array are shown in Table 3.

The spatial swath contains 1024 pixels and the spectral dispersing direction utilizes 512 pixels effectively.

The quantum efficiency of the camera product is shown in Figure 14.

Table 3: Focal plane array specifications.

Parameter	Value
Active resolution	1024 × 1024 pixels
Pixel	7.4 um
Frame Rate (frames/s)	120
Responsivity	30 DN/(nJ/cm^2)
Data format	8 bit
Dynamic range	50 dB
Mass	<175 g
Size	44 × 44 × 44 mm
Power supply	12 V to 15 V DC
Power dissipation	<3 W

6. Implementation

The final hyperspectral imaging spectrometer is designed as Figure 15. And the instrument is shown in Figure 16. The total volume of the instrument is 90 mm × 120 mm × 260 mm, and the weight is 1.7 kg.

We tested the hyperspectral imaging spectrometer by acquiring the spectrum and the image of a black textile painting two butterflies before the flight test. Since the focal plane of the telescope is corresponding to the infinity and the position of the telescope is fixed by glue to adapt to the vibration of the airplane, the image of the butterflies is a little obscured, as is shown in Figure 17. The textile is illuminated by a halogen lamp.

7. Flight Test

The flight experiment was accomplished at meridiem in a sunshiny day. The image shown in Figure 18 is composed by the red, blue, and green spectrums without other processing.

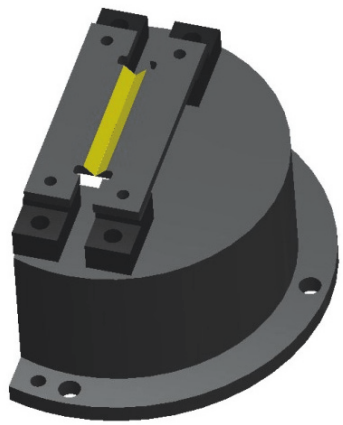

Figure 13: The slit accomplished by two blades.

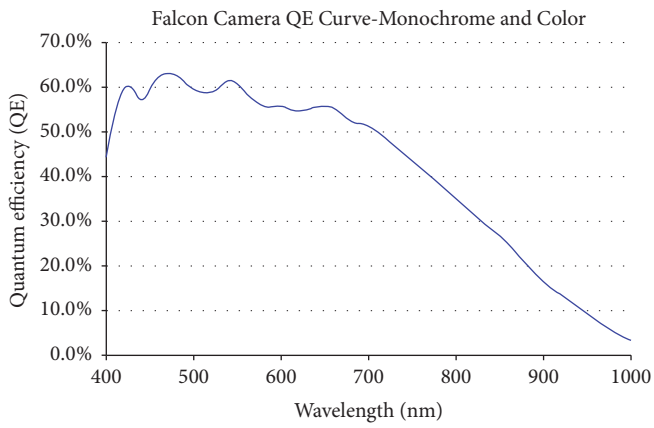

Figure 14: The quantum efficiency of the DALSA camera.

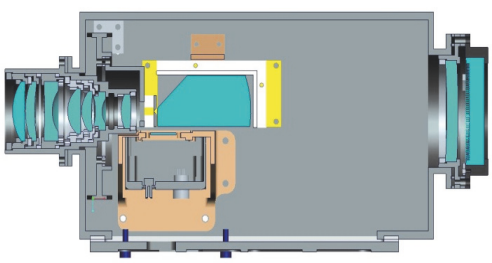

Figure 15: Diagram of the final hyperspectral imaging spectrometer.

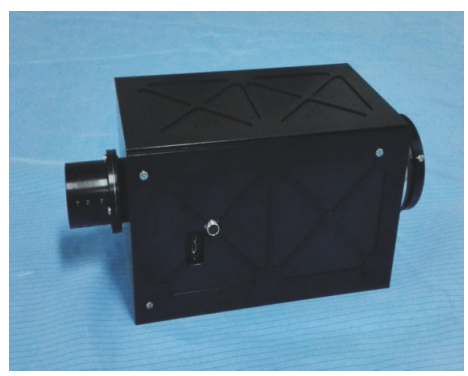

Figure 16: The compact hyperspectral imaging spectrometer.

The hyperspectral datacube acquired is shown in Figure 19. And the typical object spectrums are given. The spectral curves are obtained from the object of the blue roof, the red roof, the bared soil, and the green wheat.

It should be declared that there is a small dust falling on the slit of the spectrometer without knowing. Thus a line of pixels is blocked to receive the light of the ground, and a dark line is generated in the color image and the hyperspectral image.

8. Conclusions

In this paper, a portable hyperspectral imaging spectrometer is designed and implemented. The spectral resolution of the instrument is of 1.6 nm in the spectral range of 450 nm to 850 nm; the spatial resolution is of 0.22 mrad instantaneous FOV in the range of 6.57 degrees. The total volume of the

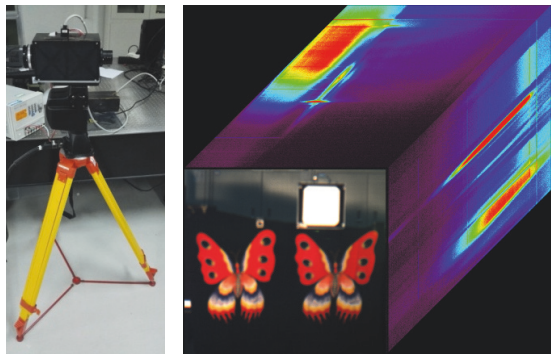

Figure 17: Test of the hyperspectral imaging spectrometer in lab.

Figure 18: The image composed by the red, blue, and green spectrums without processing.

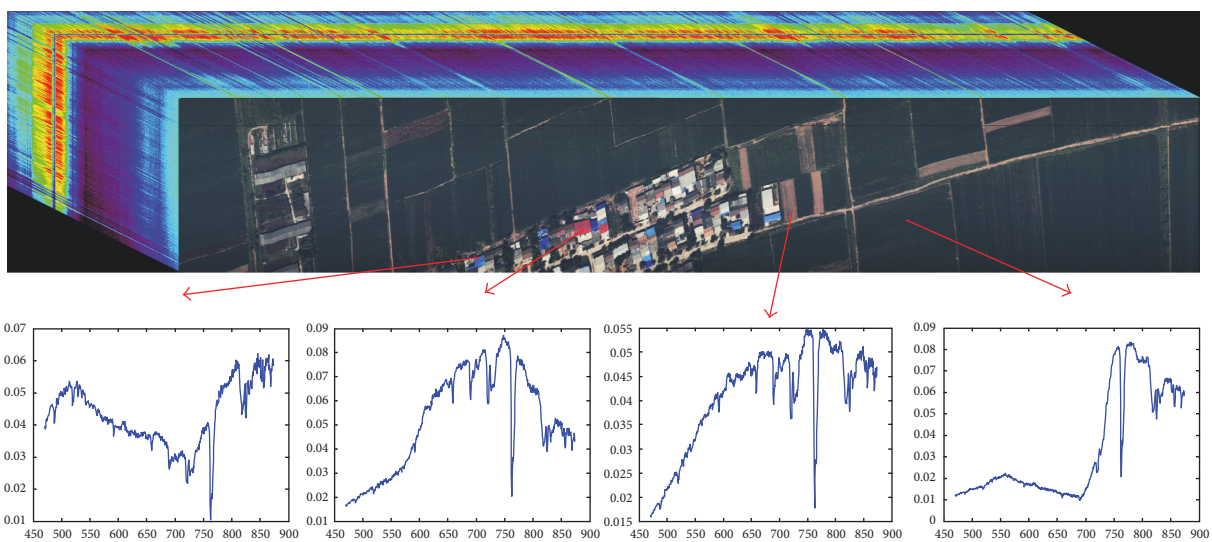

Figure 19: The hyperspectral image and the spectrums of typical objects acquired by the flight test.

instrument is 90 mm × 120 mm × 260 mm, and the weight is 1.7 kg. The hyperspectral imaging spectrometer could be used for the laboratory experiment data acquiring and remote sensing on the UAV and the CubeSat.

Conflicts of Interest

The authors declare that they have no conflicts of interest.

Acknowledgments

This work is supported by the National Natural Science Foundation of China under Grant 61501456.

References

[1] X. Prieto-Blanco, C. Montero-Orille, B. Couce, and R. De La Fuente, "Analytical design of an Offner imaging spectrometer," *Optics Express*, vol. 14, no. 20, pp. 9156–9168, 2006.

[2] P. Mouroulis, R. O. Green, and T. G. Chrien, "Design of pushbroom imaging spectrometers for optimum recovery of spectroscopic and spatial information," *Applied Optics*, vol. 39, no. 13, pp. 2210–2220, 2000.

[3] R. O. Green, M. L. Eastwood, C. M. Sarture et al., "Imaging spectroscopy and the airborne visible/infrared imaging spectrometer (AVIRIS)," *Remote Sensing of Environment*, vol. 65, no. 3, pp. 227–248, 1998.

[4] R. E. Holasek, F. P. Portigal, G. C. Mooradian et al., "HSI mapping of marine and coastal environments using the advanced

airborne hyperspectral imaging system (AAHIS)," in *Proceedings of the Algorithms for Multispectral and Hyperspectral Imagery III*, pp. 169–180, April 1997.

[5] J. Jiang, Z. Xu, J. Lin, and G. L. Liu, "Lithography-free, low-cost method for improving photodiode performance by etching silicon nanocones as antireflection layer," *Journal of Sensors*, vol. 2016, Article ID 4019864, 6 pages, 2016.

[6] R. A. Doe and S. Watchorn, "Climate-monitoring CubeSat mission (CM2): a project for global mesopause temperature sensing," in *Proceedings of the Earth Observing Systems XVI*, vol. 8153, August 2011.

[7] R. L. Staehle, B. Anderson, B. Betts et al., "Interplanetary CubeSats: opening the solar system to a broad community at lower cost," *Journal of Small Satellites (JOSS)*.

[8] G. Swenson, P. Thakker, F. Kamalabadi, M. Frank, V. Coverstone, and H. Voss, "Optical sensing of atmospheric emissions with Cubesats and Nanosats," in *Proceedings of the Sensors and Systems for Space Applications*, vol. 6555, 655506, April 2007.

[9] S. Hu, G. H. Goldman, and C. C. Borel-Donohue, "Detection of unmanned aerial vehicles using a visible camera system," *Applied Optics*, vol. 56, no. 3, pp. B214–B221, 2017.

[10] J. Dyson, "Unit magnification optical system without seidel aberrations," *Journal of the Optical Society of America*, vol. 49, no. 7, 1959.

[11] D. W. Warren, D. J. Gutierrez, and E. R. Keim, "Dyson spectrometers for high-performance infrared applications," *Optical Engineering*, vol. 47, no. 10, article 103601, 2008.

[12] P. Mouroulis, R. O. Green, and D. W. Wilson, "Optical design of a coastal ocean imaging spectrometer," *Optics Express*, vol. 16, no. 12, pp. 9087–9096, 2008.

[13] W. R. Johnson, S. J. Hook, P. Mouroulis et al., "Thermal infrared spectral imager for airborne science applications," in *Proceedings of the Infrared Technology and Applications XXXV*, vol. 7298 729802-1, April 2009.

[14] R. Lucke and J. Fisher, "The Schmidt-Dyson: A fast space-borne wide-field hyperspectral imager," in *Proceedings of the Imaging Spectrometry XV*, August 2010.

[15] C. Montero-Orille, X. Prieto-Blanco, H. González-Núñez, and R. De La Fuente, "Two-wavelength anastigmatic Dyson imaging spectrometers," *Optics Letters*, vol. 35, no. 14, pp. 2379–2381, 2010.

[16] P. Mouroulis, B. E. Van Gorp, R. O. Green et al., "The portable remote imaging spectrometer (PRISM) coastal ocean sensor," *Imaging and Applied Optics Technical Digest*, 2012.

[17] W. R. Johnson, S. J. Hook, and S. M. Shoen, "Microbolometer imaging spectrometer," *Optics Letters*, vol. 37, no. 5, pp. 803–805, 2012.

[18] L. Mertz, "Concentric spectrographs," *Applied Optics*, vol. 16, no. 12, pp. 3122–3124, 1977.

[19] D. R. Lobb, "Imaging spectrometers using concentric optics," in *Proceedings of the Imaging Spectrometry III*, pp. 339–347, July 1997.

[20] M. Pantazis, B. van Gorp, O. Robert et al., "Portable remote imaging spectrometer coastal ocean sensor: design, characteristics, and first flight results," *Applied Optics*, vol. 53, no. 7, pp. 1363–1380, 2014.